A Behavioral Dynamic Nonlinear Model for Time-Interleaved ADC Based on Volterra Series

WENTAO WEI[ID], PENG YE, JINPENG SONG[ID], HAO ZENG, JIAN GAO, AND YU ZHAO

School of Automation Engineering, University of Electronic Science and Technology of China, Chengdu 611731, China

Corresponding author: Peng Ye (yepeng_uestc@163.com)

ABSTRACT The non-ideal circuit implementations cause a significant degradation in the performance of the time-interleaved analog-to-digital converter (TIADC) system. In this paper, a behavioral model for the TIADC based on Volterra series is proposed to model the dynamic nonlinearities in TIADC. The time-domain and frequency-domain expressions of the behavioral model based on hybrid Volterra series are derived first. Then, the discrete-time equivalent model is proposed by transforming the hybrid TIADC system to a discrete time one based on discrete-time Volterra series only. The derivations give a theoretical foundation to use discrete-time Volterra series to model the mixed-domain TIADC system, which makes it possible to make full use of the related existing derivations, conclusions, and methodologies on discrete-time Volterra series. We also summarize some common special cases of Volterra series to provide practical guidelines for ADC and TIADC practitioners. We present the main features of these models and their relationship with the Volterra series. The simulation and experimental results show the effectiveness of the proposed model.

INDEX TERMS Analog-to-digital converter, time-interleaved, dynamic nonlinearities, Volterra series, discrete-time equivalent model.

I. INTRODUCTION

Analog-to-digital converter (ADC) is a critical building block as well as the bottleneck in modern telecommunication systems [1]–[3]. The rapid evolution of electronics in the past few decades has pushed ADC towards higher sampling rate. Time interleaving more than one ADC is an effective way to substantially increase sampling rate beyond a certain process technology limit [4], [5]. An ideal M-channel time-interleaved ADC (TIADC) increases the effective sampling rate by a factor of M while maintains the resolution as sub-ADCs.

However, non-ideal circuit implementations cause a significant degradation in performance of TIADC system [6]–[8]. During the last few decades, a considerable amount of literature has been published on offset, gain, time, bandwidth and frequency mismatches in TIADC system [9]–[12]. Several attempts have been made to analyze these mismatches and numerous calibration methods have been proposed to compensate for them [13]–[18].

The associate editor coordinating the review of this manuscript and approving it for publication was Sara Dadras.

In recent years, researchers have shown an increased interest in nonlinear mismatches of TIADC since nonlinear distortions deteriorate the dynamic range and reduce the effective number of bits of TIADC, especially when the input frequency increases [19], [20]. The nonlinear distortions are originated from switch-induced charge injection and input signal dependent switch on-resistance in track-and-hold (T/H) stage [20] and nonlinearities of the op-amp (operational amplifier) [21]. These nonlinearities cause nonlinear and nonlinear mismatch errors in the TIADC output, which decrease the SFDR (spurious-free dynamic range) and SINAD (signal-to-noise and distortion ratio) of the TIADC system. In practice, the distortions generated by strong signals may interfere with weak signals, therefore calibration of the nonlinear mismatch errors is required. Several calibration methods have been proposed to calibrate the nonlinearity errors in recent years [21]–[26].

So far, however, there has been relatively few papers analyzing and modeling the effects of nonlinearity mismatches in TIADC. A static nonlinear model of TIADC is proposed in [23] and [25], which is based on polynomial and can model several important nonlinearities, like differential

nonlinearities (DNL) and integral nonlinearities (INL) [27]. Vogel and Kubin [28] proposed a nonlinear hybrid filter banks to model nonlinear behaviors of TIADC, and illustrated that nonlinear hybrid filter banks can be used to model offset, gain, time and nonlinear mismatch errors. Wang *et al.* [22] proposed the static and dynamic nonlinear mismatch models of TIADC, and represented the TIADC output as the sum of original signal and error signal. A behavioral model for TIADC based on Wiener model is proposed to describe the nonlinearities in TIADC system in [29] and the authors have shown that nonlinearity mismatches are a generalization of offset, gain, time and frequency mismatches. It can be shown that the model proposed in [22], [28], and [29] can all be categorized as Wiener model.

However, these models can only represent a small subset of nonlinearities in TIADC. For polynomial-based model and Wiener-based model, they can only represent static nonlinearities and dynamic nonlinearities with Wiener model structure, respectively. Volterra series is one of the most general and well-established models in nonlinear modeling problems and have found wide applications in electronic and electrical engineering, biomedical engineering, mechanical engineering, etc [30]–[32]. A considerable amount of literature has been published on Volterra series in the past few decades [33]–[35]. Polynomial and Wiener model are all special cases of Volterra series.

In this paper, we propose a behavioral model based on Volterra series to model the dynamic nonlinear behaviors in TIADC. Since TIADC is a mixed-domain system, which involves both continuous-time and discrete-time signals, the hybrid Volterra series should be used to model the nonlinearities in TIADC system. We derive the expressions of hybrid Volterra series for mixed-domain systems both in time and frequency domain, and then generalize the results from single ADC systems to TIADC systems. The nonlinear model proposed in [22], [23], [24], [28], and [29] are all special cases of our proposed model. Thus, the model proposed in this paper is a more general model than previous ones. In practical situations, the precise nonlinear model of TIADC cannot be known beforehand as prior. Therefore, the model in this paper can represent a wider range of nonlinearities than the previous models.

What's more, we propose a discrete-time equivalent model by transforming hybrid TIADC system to a discrete time one since the hybrid system is more difficult to be handled than continuous time or discrete time system. Besides, there are extensive studies on discrete time systems on Volterra series, while much less research on hybrid systems. The derivations give a theoretical foundation to use discrete-time Volterra series to model TIADC system. The proposed model makes it possible to make full use of the related existing derivations, conclusions and methodologies on discrete-time Volterra series.

We also summarize some special cases of Volterra series to provide a practical guideline for ADC and TIADC practitioners. We present the main features of these models and

their relationship with Volterra series. Guidelines on how to choose the suitable model are also provided.

The rest of this article is structured as follows. Section II provides a brief review of the fundamental theory on Volterra series. In section III, the time and frequency domain representations of hybrid Volterra series for mixed-domain systems are derived. In section IV, a discrete-time equivalent model of TIADC based on discrete-time Volterra series is proposed. Section V describes some special cases of Volterra series. Simulation and experimental results are provided in Section VI. Finally, Section VII concludes the paper.

II. THEORY OF VOLTERRA SERIES

In order to stand on a theoretical framework to analyze dynamic nonlinear behaviors of TIADC, this section gives a brief review of the fundamental theory on Volterra series.

The continuous-time Volterra series with order P can be represented as

$$y(t) = \sum_{p=0}^{P} y_p(t) \tag{1}$$

with

$$y_p(t) = \int_{-\infty}^{\infty} \cdots \int_{-\infty}^{\infty} h_p(\tau_1, \ldots, \tau_p) \prod_{j=1}^{p} x(t - \tau_j) d\tau_j \tag{2}$$

where $x(t)$, $y(t)$ are input and output of the system respectively, and $h_p(\tau_1, \ldots, \tau_p)$ denotes the pth order continuous-time Volterra kernel. It can be assumed that Volterra kernels are symmetric without any loss of generality, that is, $h_p(\tau_1, \ldots, \tau_p)$ remains unchanged when permutating the order of $\tau_1, \ldots, \tau_p$ [31].

If the pth order Volterra kernel $h_p(\tau_1, \ldots, \tau_p)$ satisfies

$$\int_{-\infty}^{\infty} \cdots \int_{-\infty}^{\infty} |h_p(\tau_1, \ldots, \tau_p)| d\tau_1 \cdots \tau_p < \infty \tag{3}$$

then the pth order generalized frequency response function (GFRF) $H_p(j\Omega_1, \cdots, j\Omega_p)$ can be defined as the multidimensional Fourier transform of $h_p(\tau_1, \ldots, \tau_p)$, which is given by [36]

$$H_p(j\Omega_1, \cdots, j\Omega_p) = \int_{-\infty}^{\infty} \cdots \int_{-\infty}^{\infty} h_p(\tau_1, \ldots, \tau_p)$$
$$\cdot e^{-j(\Omega_1 \tau_1 + \cdots + \Omega_p \tau_p)} d\tau_1 \cdots d\tau_p \tag{4}$$

Conversely, $h_p(\tau_1, \ldots, \tau_p)$ can be recovered by means of the inverse multidimensional Fourier transform

$$h_p(\tau_1, \ldots, \tau_p) = \frac{1}{(2\pi)^p} \int_{-\infty}^{\infty} \cdots \int_{-\infty}^{\infty} H_p(j\Omega_1, \cdots, j\Omega_p)$$
$$\cdot e^{j(\Omega_1 \tau_1 + \cdots + \Omega_l \tau_p)} d\Omega_1 \cdots d\Omega_p \tag{5}$$

As we stated before, the pth order Volterra kernel $h_p(\tau_1, \ldots, \tau_p)$ can be assumed symmetrical, thus the pth order GFRF $H_p(j\Omega_1, \cdots, j\Omega_p)$ also satisfies symmetrical property.

The multidimensional frequency response of $y_p(t)$ can then be expressed as [36]

$$Y_p(j\Omega_1, \cdots, j\Omega_p) = H_p(j\Omega_1, \cdots, j\Omega_p) \prod_{i=1}^{p} X(j\Omega_i) \quad (6)$$

where $X(j\Omega)$ is the one-dimensional Fourier transform of $x(t)$.

Then, the output $y_p(t)$ can be derived from multidimensional frequency response $Y_p(j\Omega_1, \cdots, j\Omega_p)$, which is given by

$$y_p(t) = \frac{1}{(2\pi)^p} \int_{-\infty}^{\infty} \cdots \int_{-\infty}^{\infty} Y_p(j\Omega_1, \cdots, j\Omega_p) \\ \cdot e^{j(\Omega_1 + \cdots + \Omega_p)t} d\Omega_1 \cdots d\Omega_p \quad (7)$$

As can be seen in (6), the frequency domain representation of the output is a p-dimensional variable, while in the time domain the output $y(t)$ are one dimensional. Thus, in order to get a more consistent relationship between frequency domain and time domain expressions, a dimensional expansion operation is required.

A new variable Ω is defined as

$$\Omega = \sum_{i=1}^{p} \Omega_i \quad (8)$$

Then we can get

$$\Omega_p = \Omega - \sum_{i=1}^{p-1} \Omega_i \quad (9)$$

By substituting (9) into (7), we can derive

$$y_p(t) = \frac{1}{(2\pi)^p} \int_{-\infty}^{\infty} \cdots \int_{-\infty}^{\infty} Y_p(j\Omega_1, \cdots, j(\Omega - \sum_{i=1}^{p-1} \Omega_i)) \\ \cdot e^{j\Omega t} d\Omega_1 \cdots d\Omega_{p-1} d\Omega \quad (10)$$

Thus, the one-dimensional frequency domain representation of pth order output $y_p(t)$ can be described by

$$Y_p(j\Omega) = \frac{1}{(2\pi)^{p-1}} \int_{-\infty}^{\infty} \cdots \int_{-\infty}^{\infty} Y_p(j\Omega_1, \cdots, j\Omega_{p-1}, j \\ \times (\Omega - \sum_{i=1}^{p-1} \Omega_i)) d\Omega_1 \cdots d\Omega_{p-1} \quad (11)$$

The output of the Volterra series can then be obtained by summing $Y_p(j\Omega)$ from 0 to P, which is given by

$$Y(j\Omega) = \sum_{p=0}^{P} Y_p(j\Omega) \quad (12)$$

Now the system output $y(t)$ can be described by inverse Fourier transform given below just as in linear time invariant (LTI) systems with

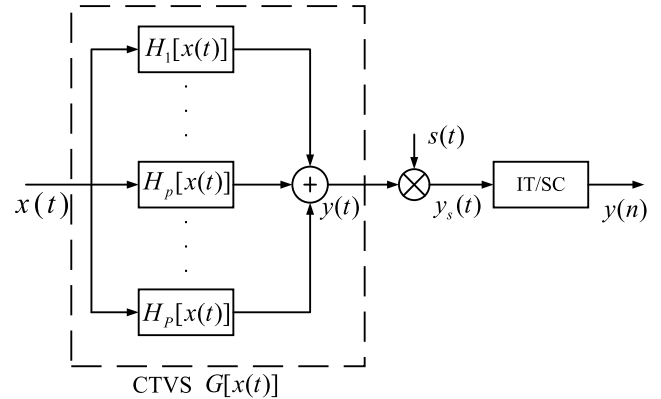$$y(t) = \frac{1}{2\pi} \int_{-\infty}^{\infty} Y(j\Omega) e^{j\Omega t} d\Omega \quad (13)$$

FIGURE 1. The diagram of the hybrid Volterra series for single ADC system.

The time and frequency domain expressions for discrete-time Volterra series have also been fully studied in the literature [36].

Volterra series can not only be seen as the generalization of Taylor series from static nonlinear systems to dynamic nonlinear systems, but also can be regarded as the extension of convolution function in LTI systems to nonlinear time-invariant systems. It is appropriate to use Volterra series as the mathematical model of TIADC.

III. HYBRID VOLTERRA SERIES FOR MIXED-DOMAIN SYSTEMS

In the previous section, the time and frequency domain representations of Volterra series have been given. However, TIADC is a mixed-domain system, i.e. the input is a continuous-time signal, while the output is a discrete-time signal. Thus, the relationship between input and output cannot be described using either standard continuous-time Volterra series or discrete-time Volterra series. In this section, we will derive the hybrid Volterra series expressions for the mixed-domain systems, and then generalize the results from single ADC systems to TIADC systems.

A. MODELING OF ADC USING HYBRID VOLTERRA SERIES
In this subsection, we will derive the hybrid Volterra series for single ADC systems both in time and frequency domain.

The diagram of the single ADC system model is shown in Fig.1. The analog input signal $x(t)$ passes through the continuous-time Volterra series (CTVS) with order P to generate output $y(t)$ as

$$y(t) = G[x(t)] = H_1[x(t)] + H_2[x(t)] + \cdots + H_P[x(t)] \quad (14)$$

where $H_p[x(t)]$ is the p-th order Volterra operator [31], which is given by

$$H_p[x(t)] = y_p(t) \quad (15)$$

as in (2) and $G[x(t)]$ is denoted as the CTVS function.

Assuming system output $y(t)$ is sampled with sampling period of T_s, hence the sampled output $y_s(t)$ is obtained by

multiplying $y(t)$ by the Dirac pulse train, i.e.

$$y_s(t) = y(t)s(t) \tag{16}$$

where

$$s(t) = \sum_{k=-\infty}^{\infty} \delta(t - kT_s) \tag{17}$$

The sampled output $y_s(t)$ propagates through an impulse-train-to-discrete-time-sequence converter (IT/SC) [37] to obtain the digital output $y(n)$. Assuming the resolution of ADC is high enough, we neglect the quantization effects.

According to multiplication property of the Fourier transform, the multiplication in the time domain corresponds to the convolution in the frequency domain [37]. Thus, the frequency response of $y_s(t)$ can be described by the following relationship

$$Y_s(j\Omega) = \frac{1}{2\pi} \int_{-\infty}^{\infty} Y(j\Theta)S(j(\Omega - \Theta))d\Theta \tag{18}$$

where $Y(j\Omega)$ is the Fourier transform of $y(t)$ and $S(j\Omega)$ is the Fourier transform of the Dirac pulse train, which is given by

$$S(j\Omega) = \frac{2\pi}{T_s} \sum_{k=-\infty}^{\infty} \delta(\Omega - k\frac{2\pi}{T_s}) \tag{19}$$

With (18) and (19), the sampled output of CTVS $Y_s(j\Omega)$ can be derived as

$$
\begin{aligned}
Y_s(j\Omega) &= \frac{1}{T_s} \sum_{k=-\infty}^{\infty} \sum_{p=0}^{P} Y_p(j(\Omega - k\frac{2\pi}{T_s})) \\
&= \frac{1}{T_s} \frac{1}{(2\pi)^{p-1}} \sum_{k=-\infty}^{\infty} \sum_{p=0}^{P} \int_{-\infty}^{\infty} \cdots \int_{-\infty}^{\infty} \\
&\quad \times Y_p(j\Omega_1, \cdots, j(\Omega - \sum_{i=1}^{p-1}\Omega_i - k\frac{2\pi}{T_s})) \\
&\quad \times d\Omega_1 \cdots d\Omega_{p-1}
\end{aligned}
\tag{20}
$$

where $Y_p(j\Omega_1, \cdots, j\Omega_p)$ and $Y_p(j\Omega)$ are defined in (6) and (11) respectively.

B. MODELING OF TIADC USING HYBRID VOLTERRA SERIES

In section A, we have derived the hybrid Volterra series for single ADC systems both in time and frequency domain. In this subsection, we generalize the results to TIADC systems.

An M channel TIADC model using hybrid Volterra series is depicted in Fig.2. The analog input signal $x(t)$ is fed to the mth ($m = 0, \ldots, M-1$) CTVS function $G_m[x(t)]$ as denoted in (14) to obtain the $y_m(t)$. Assuming the aggregate sampling rate is $f_s(= 1/T_s)$. Then the sampled output $y_{m,s}(t)$ is obtained by multiplying $y_m(t)$ by $s_m(t)$, where

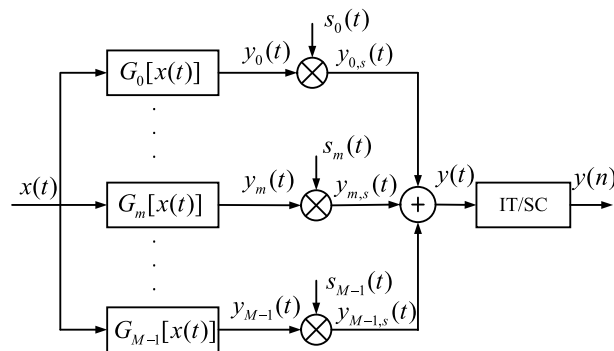$$s_m(t) = \sum_{k=-\infty}^{\infty} \delta(t - mT_s - kMT_s) \tag{21}$$

FIGURE 2. An M channel TIADC model based on Hybrid Volterra series.

Therefore, the output of mth channel can be written as

$$y_{m,s}(t) = \sum_{k=-\infty}^{\infty} G_m[x(t)]\delta(t - mT_s - kMT_s) \tag{22}$$

Then the sampled output of the TIADC system $y(t)$ can be obtained by adding outputs of M channels

$$y(t) = \sum_{m=0}^{M-1} y_{m,s}(t) \tag{23}$$

The $y(t)$ are followed by the IT/SC block to get the final digital output $y(n)$.

Following the same procedure as single ADC system, the frequency domain representation of mth channel output $y_{m,s}(t)$ is given by

$$Y_{m,s}(j\Omega) = \frac{1}{2\pi} \int_{-\infty}^{\infty} Y_m(j\Theta)S_m(j(\Omega - \Theta))d\Theta \tag{24}$$

where $Y_m(j\Omega)$ is the Fourier transform of the $y_m(t)$, which has the same expression as (14) only by changing $G[x(t)]$ with mth channel CTVS function $G_m[x(t)]$.

The $S_m(j\Omega)$ can be obtained by using Poisson summation formula. The Poisson summation formula is expressed as

$$\sum_{k=-\infty}^{\infty} \delta(t - kT) = \frac{1}{T} \sum_{k=-\infty}^{\infty} e^{j2\pi kt/T} \tag{25}$$

By replacing t with $t - mT_s$ and T with MT_s, (25) can be expressed as

$$
\begin{aligned}
s_m(t) &= \sum_{k=-\infty}^{\infty} \delta(t - mT_s - kMT_s) \\
&= \frac{1}{MT_s} \sum_{k=-\infty}^{\infty} e^{j2\pi k(t-mT_s)/MT_s}
\end{aligned}
\tag{26}
$$

By taking the continuous-time Fourier transform to (26), the $S_m(j\Omega)$ can be written as

$$S_m(j\Omega) = \frac{2\pi}{MT_s} \sum_{k=-\infty}^{\infty} e^{-j2\pi k\frac{m}{M}}\delta(\Omega - k\frac{2\pi}{MT_s}) \tag{27}$$

Combining (27) with (24), the $Y_{m,s}(j\Omega)$ can then be derived as

$$
\begin{aligned}
Y_{m,s}(j\Omega) &= \frac{1}{MT_s} \sum_{k=-\infty}^{\infty} e^{-j2\pi k \frac{m}{M}} Y_m(j(\Omega - k\frac{2\pi}{MT_s})) \\
&= \frac{1}{MT_s} \sum_{k=-\infty}^{\infty} \sum_{p=0}^{P} e^{-j2\pi k \frac{m}{M}} Y_{m,p}(j(\Omega - k\frac{2\pi}{MT_s})) \\
&= \frac{1}{MT_s} \frac{1}{(2\pi)^{p-1}} \sum_{k=-\infty}^{\infty} \sum_{p=0}^{P} \int_{-\infty}^{\infty} \cdots \int_{-\infty}^{\infty} \\
&\quad \times e^{-j2\pi k \frac{m}{M}} Y_{m,p}(j\Omega_1, \cdots, j(\Omega - \sum_{i=1}^{p-1} \Omega_i - k\frac{2\pi}{MT_s})) \\
&\quad \times d\Omega_1 \cdots d\Omega_{p-1}
\end{aligned}
\tag{28}
$$

The frequency domain representation of $y(t)$ can then be obtained by summing all $Y_{m,s}(j\Omega)$ together, i.e.

$$
Y(j\Omega) = \sum_{m=0}^{M-1} Y_{m,s}(j\Omega)
\tag{29}
$$

IV. DISCRETE-TIME NONLINEAR EQUIVALENT MODEL OF TIADC

In the previous section, we have derived the TIADC model using hybrid Volterra series. However, hybrid systems are more difficult to be handled than continuous time or discrete time systems. What's more, there are extensive studies on continuous time or discrete time systems on Volterra series, while much less research on hybrid systems. Thus, in order to make full use of the related existing derivations, conclusions and methodologies on Volterra series, we will derive the discrete-time equivalent nonlinear model of TIADC based on Volterra series.

In [38], the author has shown that although nonlinearity produces a higher frequency range than input signal, it is sufficient to sample at twice the maximum frequency of the input signal rather than the output signal. Thus, we can assume a band-limited analog signal $x(t)$ which satisfies

$$
X(j\Omega) = 0, \ |\Omega| \geq B; \quad B \leq \frac{\pi}{T_s}
\tag{30}
$$

where $X(j\Omega)$ is the Fourier transform of $x(t)$, then we can get

$$
X(e^{j\omega}) = \frac{1}{T_s} X(j\Omega), \quad \omega \in [-\pi, \pi]
\tag{31}
$$

where

$$
\omega = \Omega T_s
\tag{32}
$$

and $X(e^{j\omega})$ is the discrete-time Fourier transform of the digital signal $x(n)$, which is the sampled output of $x(t)$ with

$$
x(n) = x(nT_s)
\tag{33}
$$

Assuming the pth order discrete-time Volterra transfer function of mth channel $H_{m,p}(e^{j\omega_1}, \ldots, e^{j\omega_p})$ is the 2π periodic
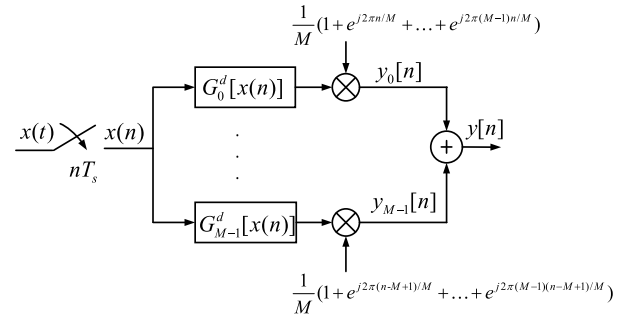

FIGURE 3. Discrete-time nonlinear equivalent TIADC model with *M* channels for band limited input signal *x(t)*.

extended version of the band limited continuous-time GFRF, i.e.

$$
H_{m,p}(e^{j\omega_1}, \ldots, e^{j\omega_p}) = H_{m,p}(j\frac{\omega_1}{T_s}, \ldots, j\frac{\omega_p}{T_s}),
$$
$$
(-\pi \leq \omega_i \leq \pi)
\tag{34}
$$

It should be noted that there are several representations of discrete-time Volterra transfer function, like $H_{m,p}^d(f_1, \ldots, f_p)$ in [38], $H_{m,p}(j\omega_1, \ldots, j\omega_p)$ in [36] and etc. In this paper, we use $H_{m,p}(e^{j\omega_1}, \ldots, e^{j\omega_p})$ to represent discrete-time Volterra transfer function, which is a generalization of the one dimensional discrete-time transfer function $H(e^{j\omega})$.

According to (6) and (31), the discrete-time multidimensional frequency response of mth channel can then be written as

$$
Y_{m,p}(e^{j\omega_1}, \ldots, e^{j\omega_n}) = T_s^p H_{m,p}(e^{j\omega_1}, \ldots, e^{j\omega_p}) \prod_{i=1}^{p} X(e^{j\omega_i})
\tag{35}
$$

Combining (35) with (28), the frequency response of discrete-time output $y_m(n)$ of mth channel is given by

$$
\begin{aligned}
Y_m(e^{j\omega}) &= \frac{1}{MT_s} \sum_{k=0}^{M-1} e^{-j2\pi k \frac{m}{M}} Y_m(e^{j(\omega - k\frac{2\pi}{M})}) \\
&= \frac{1}{M} (\frac{T_s}{2\pi})^{p-1} \sum_{k=0}^{M-1} \sum_{p=0}^{P} e^{-j2\pi k \frac{m}{M}} \int_{-\pi}^{\pi} \cdots \int_{-\pi}^{\pi} \\
&\quad \times H_{m,p}(e^{j\omega_1}, \ldots, e^{j(\omega - \sum_{i=1}^{p-1} \omega_i - k\frac{2\pi}{M})}) \\
&\quad \times \prod_{i=1}^{p-1} X(e^{j\omega_i}) X(e^{j(\omega - \sum_{i=1}^{p-1} \omega_i - k\frac{2\pi}{M})}) d\omega_1 \cdots d\omega_{p-1}
\end{aligned}
\tag{36}
$$

The frequency domain representation of digital output signal $y(n)$ can then be obtained by

$$
Y(e^{j\omega}) = \sum_{m=0}^{M-1} Y_m(e^{j\omega})
\tag{37}
$$

Next, we will derive the time-domain representations of discrete-time nonlinear equivalent TIADC model based on Volterra series, which is depicted in Fig.3.

First, we will give the formula of standard discrete-time Volterra series. The discrete-time multidimensional Fourier transform of pth order output $y_p(n)$ in general Volterra series is given by

$$Y_p(e^{j\omega_1}, \ldots, e^{j\omega_p}) = H_p(e^{j\omega_1}, \ldots, e^{j\omega_p}) \prod_{i=1}^{p} X(e^{j\omega_i}) \quad (38)$$

Compared (38) with (35), the pth order discrete-time equivalent GFRF of mth channel can be described by

$$H_{m,p}^d(e^{j\omega_1}, \ldots, e^{j\omega_n}) = T_s^p H_{m,p}(e^{j\omega_1}, \ldots, e^{j\omega_n}) \quad (39)$$

where $H_{m,p}(e^{j\omega_1}, \ldots, e^{j\omega_n})$ is given in (34).

The time-domain representation of the discrete-time equivalent Volterra kernels can be obtained by taking inverse Fourier transform of (39) as

$$h_{m,p}(k_1, \cdots, k_n) = \frac{1}{(2\pi)^p} \int_{-\pi}^{\pi} \cdots \int_{-\pi}^{\pi} H_{m,p}^d(e^{j\omega_1}, \ldots, e^{j\omega_p})$$
$$\cdots e^{j(\omega_1 k_1 + \cdots + \omega_p k_p)} d\omega_1 \cdots d\omega_p \quad (40)$$

Define mth channel discrete-time Volterra series (DTVS) function $G_m^d[x(n)]$ in Fig.3 as

$$G_m^d[x(n)] = \sum_{p=0}^{P} \sum_{k_1=-\infty}^{\infty} \cdots \sum_{k_p=-\infty}^{\infty} h_{m,p}(k_1, \cdots, k_p) \prod_{i=1}^{p} x(n-k_i) \quad (41)$$

Then the output $y_m(n)$ of mth channel is given by

$$y_m(n) = \frac{1}{M} \sum_{k=0}^{M-1} e^{jk\frac{2\pi}{M}(n-m)} G_m^d[x(n)]$$
$$= \frac{1}{M} \sum_{p=0}^{P} \sum_{k=0}^{M-1} \sum_{k_1=-\infty}^{\infty} \cdots \sum_{k_p=-\infty}^{\infty} e^{jk\frac{2\pi}{M}(n-m)}$$
$$\cdot h_{m,p}(k_1, \cdots, k_p) \prod_{i=1}^{l} x(n-k_i) \quad (42)$$

The output $y(n)$ can then be written as

$$y(n) = \sum_{m=0}^{M-1} y_m(n) \quad (43)$$

The discrete-time equivalent model of TIADC provides the theoretical foundation to use discrete-time Volterra series to model nonlinear behaviors in TIADC if input signal is band-limited. In many cases, there is no need to obtain neither the continuous-time GFRF nor discrete-time GFRF of Volterra series explicitly.

V. SPECIAL CASES OF VOLTERRA SERIES
The Volterra series is one of the most general models of nonlinear systems. However, the coefficients of the Volterra series expand rapidly with nonlinear order and memory. There is no need to use full Volterra series in most practical situations. Besides, the large number of coefficients also cause the ill-conditioned problem in identification. So in

practice, we would like to choose some special cases of Volterra series to approximate the nonlinear system.

In this section, we provide some simpler special cases of Volterra series, all of which have found wide applications in practical engineering, such as electronic and electrical engineering, mechanical engineering, control engineering, etc. These models either have simpler structures and fewer parameters than general Volterra series, or can be easily identified and compensated. The price paid for these advantages is that there is fewer physical process can be described by these simplified models. In practice, there are several different architectures of TIADC involving different manufacture process. Besides, nonlinearity in TIADC is not the original intention of ADC designers, and it is a non-ideal phenomenon essentially. Thus, the precise nonlinear model structure of TIADC cannot be known beforehand as prior in practical situations. This section will introduce the main features of these models and their relationship with Volterra series to provide practical guidelines for ADC and TIADC practitioners.

A. POLYNOMIAL MODEL
According to the Weierstrass approximation theorem [39], every continuous function defined on a closed interval $[a, b]$ can be uniformly approximated as closely as desired by a polynomial function. Thus, the polynomial model is the most widely used static nonlinear model, which is given by

$$y(n) = \sum_{p=0}^{P} a_p x(n)^p \quad (44)$$

where P is the order of the polynomial model and $x(n)$, $y(n)$ are the input and output of polynomial model respectively. According to the definition of Volterra series, the polynomial model can be obtained by taking

$$h_p(k_1, \cdots, k_p) = a_p \delta(k_1) \cdots \delta(k_p) \quad (45)$$

From (44), it can be seen that output of the polynomial model is only dependent on the current input, which implies that the past and future input cannot affect the current output. This is a strong assumption that there are rare systems in practice can meet this requirement since most systems have memory effects to some extent. Thus polynomial model finds limited use in practical situations.
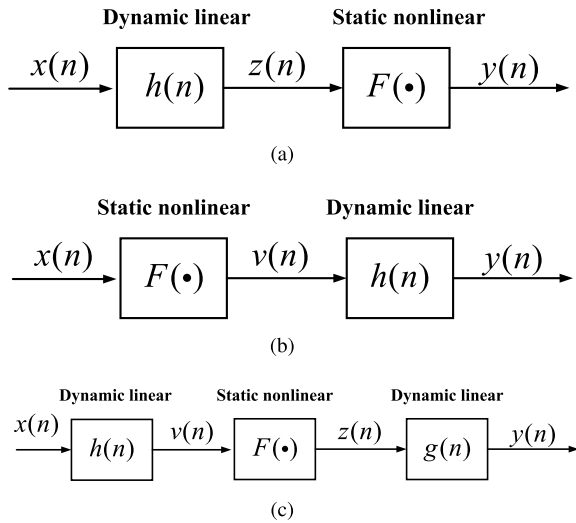
B. WIENER MODEL
Wiener model consists of a dynamic linear system followed by a static nonlinear system, which is shown in Fig.4(a) [40]. The relationship of Wiener model can be described by

$$y(n) = F(z(n)) \quad (46)$$

where $z(n)$ is the output of the dynamic linear system, which is given by

$$z(n) = \sum_{k=\infty}^{\infty} h(k)x(n-k) \quad (47)$$

Dynamic linear   **Static nonlinear**

(a)

Static nonlinear   **Dynamic linear**

(b)

Dynamic linear   **Static nonlinear**   **Dynamic linear**

(c)

FIGURE 4. **Some special cases of Volterra series. (a) Wiener model. (b) Hammerstein model. (c) Wiener-Hammerstein model.**

with $x(n)$ as the input and $h(n)$ as the impulse response of the system. $F(\cdot)$ is the nonlinear function of the static nonlinear system, and is usually assumed to be the polynomial function. Thus the output of Wiener model with polynomial order P is given by

$$y(n) = \sum_{p=0}^{P} a_p \left[\sum_{k=-\infty}^{\infty} h(k)x(n-k) \right]^p \quad (48)$$

By comparing with the definition of discrete-time Volterra series, Wiener model can be obtained by taking

$$h_p(k_1, \cdots, k_p) = a_p h(k_1) \cdots h(k_p), p = 1, \cdots, P \quad (49)$$

Compared with polynomial model, Wiener model takes the dynamic characteristic of the system into account, thus can be used to describe the dynamic nonlinear systems. However, the output of Wiener model is nonlinearly dependent on the coefficients $h(k)$, which makes the identification of Wiener model become quite complicated since nonlinear optimization should be adopt.

C. HAMMERSTEIN MODEL

The Hammerstein model has a similar structure as Wiener model but with a static nonlinear system followed by a dynamic linear system, as shown in Fig.4 (b) [41]. The expression for Hammerstein model is given by

$$y(n) = \sum_{k=-\infty}^{\infty} h(k)v(n-k) \quad (50)$$

where $v(n)$ is the output of nonlinear system, which is represented as

$$v(n) = F(x(n)) = \sum_{p=0}^{P} a_p x(n)^p \quad (51)$$

The $x(n)$, $y(n)$, $F(\cdot)$, a_p are just as defined in Wiener model. The relationship between Hammerstein model and Volterra

series can be represented as

$$h_p(k_1, \cdots, k_p) = \begin{cases} a_p h(k), & k_1 = k_2 = \cdots = k_p = k \\ 0, & otherwise \end{cases} \quad (52)$$

For Hammerstein model, only the diagonal components of the Volterra kernel have value not equal to zero. The Hammerstein model has a desirable features that the output depend linearly on the parameters $a_p h(k)$, thus can be solved using least-squares method. However, the Hammerstein model can represent much less physical process in practice than Wiener model due to its structure.

It should be noted that Hammerstein model and Wiener model constitute mutual inverse. Thus, if a dynamic nonlinear system can be modeled by Wiener model, the nonlinearity can be compensated by Hammerstein model, and vice versa.

D. WIENER-HAMMERSTEIN MODEL

The structure of Wiener-Hammerstein model is shown in Fig.4 (c) [42]. It is a combination of Wiener and Hammerstein model that a static nonlinear system is preceded and followed by the dynamic linear system. The relationship can be represented as

$$y(n) = \sum_{k=-\infty}^{\infty} g(k)z(n-k) \quad (53)$$

$$z(n) = F(v(n)) = \sum_{p=0}^{P} a_p v(n)^p \quad (54)$$

$$v(n) = \sum_{k=-\infty}^{\infty} h(k)x(n-k) \quad (55)$$

where $v(n)$ is the output of first LTI block, $z(n)$ is the output of static nonlinear system, and $h(k)$, $g(k)$ are impulse response of the first and second linear systems respectively.

The relationship between Volterra series and Wiener-Hammerstein model is given by

$$h_p(k_1, \cdots, k_p) = a_p \sum_{k=-\infty}^{\infty} g(k)h(k_1 - k) \cdots h(k_p - k),$$

$$(p = 1, \cdots, P) \quad (56)$$

Wiener-Hammerstein model can describe a much wider physical process than Wiener and Hammerstein model and has found wide applications in nonlinear systems. However, it also has the same undesired attribute like Wiener model that output is a nonlinear function of the parameters.

E. MEMORY POLYNOMIAL

Memory polynomial is a widely used model in power amplifiers, which has proven as an effective model to model nonlinear behaviors of actual power amplifiers [43], [44]. The expression for memory polynomial model is given as

$$y(n) = \sum_{p=0}^{P} \sum_{k=0}^{K-1} a_{pk} x(n-k)^p \quad (57)$$

where P and K are the order and memory length of memory polynomial model respectively.

The relationship between memory polynomial model and Volterra series can be represented as

$$h_p(k_1, \cdots, k_p) = \begin{cases} a_{pk}, & k_1 = k_2 = \cdots = k_p = k \\ 0, & otherwise \end{cases} \quad (58)$$

Compared with (49), it can be seen that Hammerstein is a special case of memory polynomial. In [44], the authors have proven that memory polynomial is a parallel Hammerstein model. The memory polynomial not only incorporates memory effects into the static nonlinear system, but also is easier to be identified since the output has linear relationship with coefficients a_{pk}. The parameters of memory polynomial model can be obtained by any least-squares type of algorithm.

F. OTHER VARIANTS OF VOLTERRA SERIES

Apart from the nonlinear models we mentioned above, there are several other variants of Volterra series, like generalized memory polynomial model [45], dynamic deviation model [46], envelope-memory polynomial model, and etc. Interested readers can find more details of these models in the literature [47].

VI. SIMULATION AND EXPERIMENTAL RESULTS

A. SIMULATION RESULTS

In this section, the numerical simulations with MATLAB are performed to prove the validity of the proposed model.

We have investigated a four channel TIADC with aggregate sampling rate of 5GSPS. The model of each channel is assumed to follow a Wiener-Hammerstein structure (see Fig.4(c)), since Wiener-Hammerstein model can represent a large class of dynamic nonlinear systems. In TIADC system, each channel passes through Wiener-Hammerstein model with different parameters, which would cause nonlinear mismatch errors in the output. This model can describe offset, linear and higher order nonlinear mismatch errors in the TIADC system.

The transfer functions of the first LTI block for four channels are set as

$$H_0(z) = 1 + 0.02z^{-1} + 0.05z^{-2} \quad (59)$$
$$H_1(z) = 1 - 0.01z^{-1} + 0.03z^{-2} \quad (60)$$
$$H_2(z) = 1 + 0.02z^{-1} + 0.01z^{-2} \quad (61)$$
$$H_3(z) = 1 - 0.03z^{-1} + 0.04z^{-2} \quad (62)$$

respectively.

In practice, TIADC is a weak nonlinear system and only second and third order nonlinearities dominant the nonlinear behaviors of TIADC system [20]. Thus, the coefficients of the static nonlinear blocks for four channels are set as $a_{m,0} = [-0.002, 0.003, 0.001, -0.001]$, $a_{m,1} = [1.02, 0.96, 1.010, 0.989]$, $a_{m,2} = [0.02, -0.01, 0.03, -0.05]$, and $a_{m,3} = [0.02, 0.03, -0.03, 0.01]$. We also add a weak fifth nonlinear distortions with parameters

$a_{m,5} = [0.001, 0.002, 0.003, -0.002]$ to demonstrate the effectiveness of our proposed model.

The transfer functions of LTI block after static nonlinear block are set as

$$G_0(z) = 1 - 0.02z^{-1} - 0.12z^{-2} \quad (63)$$
$$G_1(z) = 1 + 0.01z^{-1} - 0.11z^{-2} \quad (64)$$
$$G_2(z) = 1 - 0.01z^{-1} - 0.03z^{-2} \quad (65)$$
$$G_3(z) = 1 + 0.02z^{-1} - 0.01z^{-2} \quad (66)$$

respectively. We also add white Gaussian noise to the TIADC output to simulate noise generated in practical situations.

Most existing literature on TIADC nonlinear behaviors are based on polynomial model [23]–[25], which can only model static nonlinearities in TIADC system. We will compare Volterra-based model with polynomial-based model next. The nonlinear order of these two models are both third order, which can model nonlinearities up to third order. The memory length of Volterra series is taken as 4.

In order to show the modeling performance of the two models, the identification of the parameters should be performed firstly. Since the output of the two models are both linear dependent on their parameters, they can all be expressed as the following form

$$Y = \Phi b \quad (67)$$

with $\Phi = [W_0 X, \cdots, W_{M-1} X]$ and $Y = [y(1), \cdots, y(N)]^T$, where $y(n)$ is the TIADC output at instant n and N is the length of date used for identification. W_m is a diagonal matrix $(m = 0, \cdots, M - 1)$

$$W_m = \begin{bmatrix} \sum_{k=0}^{M-1} e^{jk\frac{2\pi}{M}(1-m)} & \cdots & 0 \\ \vdots & \ddots & \vdots \\ 0 & \cdots & \sum_{k=0}^{M-1} e^{jk\frac{2\pi}{M}(N-m)} \end{bmatrix} \quad (68)$$

b is the coefficients of the model parameters and X is the associated input matrix.

For polynomial-based model, b is defined as

$$b = [a_0^T, \ldots, a_{M-1}^T]^T \quad (69)$$

where

$$a_m = [a_{m,0}, \ldots, a_{m,P}]^T \quad (70)$$

with $a_{m,p}$ as the polynomial parameters of mth channel.

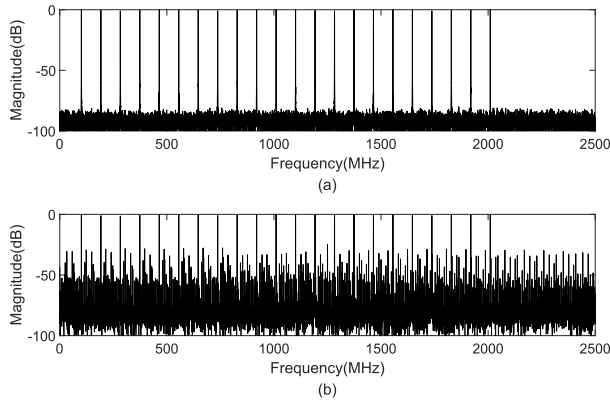For Volterra-based model, b is defined as

$$b = [h_0^T, \ldots, h_{M-1}^T]^T \quad (71)$$

where

$$h_m = [h_{m,0}^T, \ldots, h_{m,P}^T]^T \quad (72)$$

with $h_{m,p}$ as the coefficients associated with pth order Volterra kernel of mth channel.

FIGURE 5. Spectrum of the input signal and output of a four channel TIADC with nonlinearity obey Wiener-Hammerstein model structure. (a) Spectrum of the input signal (b) Spectrum of TIADC output.

FIGURE 6. A sample of time-domain waveforms of TIADC output with dynamic nonlinear distortions and fitted output with polynomial-based model and Volterra-based model. The mark 'x' represents the sampled output TIADC system with Wiener-Hammerstein model. The blue line depicts the fitted output with polynomial-based model and red line represents the fitted output with Volterra-based model.

The matrix X is defined as

$$X = \begin{bmatrix} x^0(1) & x^1(1) & \cdots & x^P(1) \\ x^0(2) & x^1(2) & \cdots & x^P(2) \\ \vdots & \vdots & \ddots & \vdots \\ x^0(N) & x^1(N) & \cdots & x^P(N) \end{bmatrix} \quad (73)$$

with $x^p(n)$ as the pth order term corresponds to the pth order model coefficients, where

$$x^p(n) = x(n)^p \quad (74)$$

for polynomial-based model and

$$x^p(n) = [x(n)^p, x(n)^{p-1}x(n-1), x(n)^{p-1}x(n-2), \cdots] \quad (75)$$
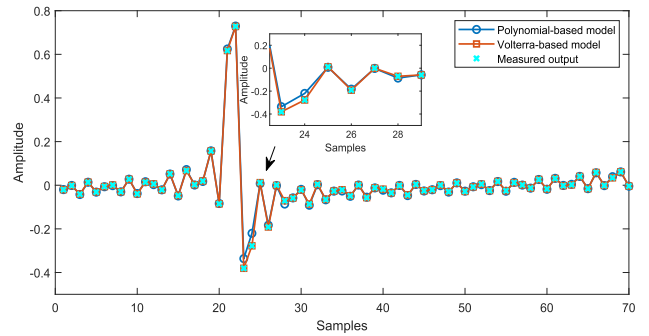
for Volterra-based model.

The parameters of the models can then be solved using least-squares method, which is given by

$$\hat{b} = (\Phi^H \Phi)^{-1} \Phi^H Y \quad (76)$$

Since the dynamic nonlinear system is dependent on frequency, the input signal should cover sufficiently wide frequency range to obtain the estimated parameters of the model. Multi-tone signal is a widely applied excitation signal in ADC dynamic testing [49]. In the simulation, we use multi-tone signal as the input of the dynamic nonlinear TIADC system to investigate the nonlinear effects of TIADC.

The multi-tone signal to the TIADC system is composed of 22 uniform amplitude sinusoids with equal spaced frequencies from DC to 0.8π. The spectrum of the input signal and TIADC output signal are shown in Fig. 5. It can be seen clearly from the figure that for multi-tone input signal, there are plenty of spurious tones in the output, which substantially degrade the performance of the TIADC. The situation will become worse when the wide-band signal is applied, like WCDMA (wideband code division multiple access) signal.

In the simulation, we use 1000 samples for the identification, i.e. $N = 1000$ in (67). The parameters of the model are

solved using (76). The fitted output with chosen model is then given by

$$\hat{Y} = \Phi \hat{b} \quad (77)$$

The accuracy of the model can be assessed using NMSE (normalized mean squared error), which is defined as the power of the error vector between measured and modeled output, normalized to the measured output power [46],

$$NMSE = 10 log_{10} \left[\frac{\sum_{i=1}^{N} |y_i - \hat{y}_i|^2}{\sum_{i=1}^{N} |y_i|^2} \right] \quad (78)$$

where y_i is the measured TIADC output with nonlinearities, $\hat{y}_i$ is the fitted output with chosen model and N is the sample length used for evaluating NMSE. The NMSE of polynomial-based and Volterra-based model in the simulation are -25.36dB and -53.21dB respectively.

A sample of time-domain waveform is shown in Fig.6. The mark 'x' represents the sampled output of the TIADC system with dynamic nonlinear distortions, which follows Wiener-Hammerstein structure. The blue line depicts the fitted output with polynomial-based model and red line represents the fitted output with Volterra-based model. From the figure, it can be seen that Volterra-based model has much better modeling performance than polynomial-based model.

It can be concluded that the static polynomial model cannot model a dynamic nonlinear systems well, thus nonlinear models with memory are required in practice to model the nonlinear behaviors in TIADC system, which shows the necessity of our proposed model. What's more, it can be seen that Volterra series can model Wiener-Hammerstein model very accurately. Increasing the memory length can improve the modeling performance of nonlinear dynamic model but the complexity is also increased [32].

In practice, if we know the appropriate model of the nonlinear system beforehand, just identification of the coefficients is required. However, in most cases, the appropriate model structure cannot be known in advance, thus we need to choose
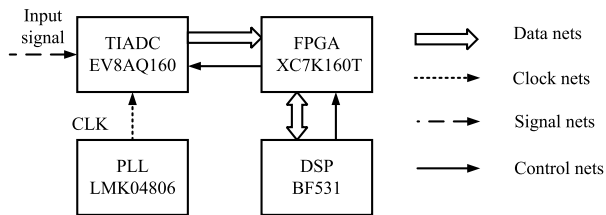
FIGURE 7. Simplified block diagram of the system hardware setup. The DUT is a commercial ADC EV8AQ160 from E2V company with aggregate sampling rate of 5GSPS. The clock signal of TIADC is generated by PLL LMK04806. The digital streams are received and stored by Kintex-7 series FPGA from Xilinx company. The DSP from Analog Devices company is responsible for system controlling and data processing.

FIGURE 8. The printed circuit board of an acquisition system with 5GSPS sampling rate. The main components of the acquisition system are composed of TIADC, PLL, FPGA and DSP.

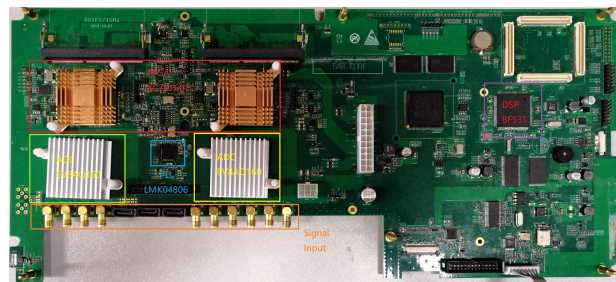FIGURE 9. Block diagram of the measurement setup.

a suitable model for the system. The strategy for model selection can be started from relatively simple model. If the chosen model cannot model nonlinear system accurately, more complex model should be chosen. For example, memory polynomial model takes only the diagonal terms of Volterra series, hence it can be chosen firstly. If memory polynomial model cannot give satisfactory results, it can be replaced by the generalized memory polynomial model, which adds cross terms of Volterra series to memory polynomial model and thus is a more complex model.

It also should be noted that in practical situations, even two models have similar modeling performance, a model that is easier to be identified can have superior advantages than models with complex identification methods. For instance, the output of Wiener model has nonlinear relationship with the coefficients, thus the nonlinear optimization methods should be applied to identify the coefficients. While for memory polynomial, generalized memory polynomial and Volterra model, the output has linear relationship with coefficients, thus can be identified using any least-squares type of algorithm.

B. EXPERIMENTAL RESULTS

The subject of this section is to show the validity of the proposed model by experimental results. The simplified block diagram of the system hardware setup is shown in Fig.7. The DUT (device under test) is a commercial ADC EV8AQ160 from E2V company, which has four 8-bit ADC cores operating in a TI manner with sampling rate 1.25GSPS for each channel and the aggregate sampling rate of 5GSPS [50]. The clock signal of TIADC is generated by PLL (phase-locked loop) LMK04806 from Texas Instruments company. The digital streams are received and stored by Kintex-7 series FPGA (field programmable gate array) from Xilinx company, which is also used for signal processing and ADC control. The DSP (digital signal processor) from Analog Devices company is responsible for system controlling and data processing. The calibration algorithm can be implemented in either FPGA or DSP. The printed circuit board of the acquisition system is shown in Fig.8.

As stated in VI.A, the excitation signal of the system should be a wide-band signal. In the simulation, we adopt multi-tone signal as the input signal. However, in practical
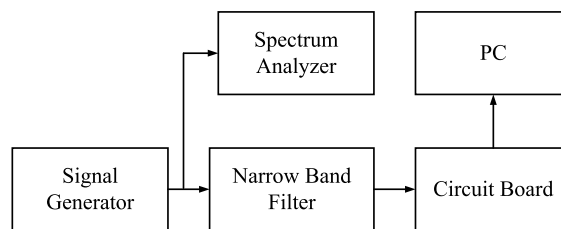
situations, even though some signal generators can generate multi-tone signals, the achievable SINAD is not high enough for testing and the intermodulation distortions cannot be filtered. Schmidt et al. [48] proposed a novel training signal by concatenating sinusoids in time, which is given by

$$x(t) = \sum_{k=1}^{K} cos(2\pi f_k t) \left[u(t - t_{ik}) - u(t - t_{fk}) \right] \quad (79)$$

where f_k is the frequency of the sinusoids, $u(t)$ is the step function, t_{ik} and t_{fk} are initial and final time instant of sinusoids k respectively. Authors have proved that this novel training signal has similar effects as multi-tone signal and demonstrated the validity of the signal in experimental results.

The test analog input signal in our experiment is generated by Rohde & Schwarz SMA100A RF signal generator. From actual measurement and datasheet of SMA100A [51], we found that it is difficult for signal generator to generate clean single-tone sinusoid in practice. In order to obtain the nonlinear behaviors of TIADC, we have to eliminate the nonlinear distortions generated by signal generator. The bandpass filters from Mini company are used for this purpose, which have excellent filter performance. According to [49], the nonlinear testing of ADC requires the utilization of large amplitude sin waves. Thus, the amplitude of the input signal after bandpass filters are all adjusted to 90% of the full scale range of the converter in every frequency. The spectrum analyzer is used for the adjustment and it can also assess the performance of the generated input signal. The block diagram and actual picture of the measurement setup are shown in Fig.9 and Fig.10, respectively.
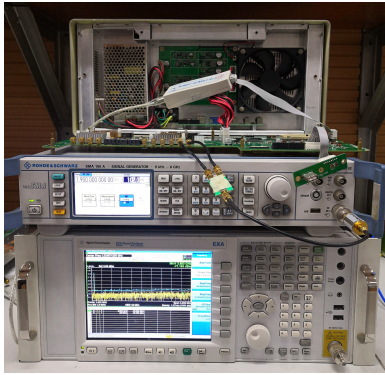
FIGURE 10. Actual picture of the measurement setup.

FIGURE 11. Output spectrum of each sub-ADC core of EV8AQ160 8-bit TIADC with 800MHz input signal. (a) Output spectrum of ADC core A (b) Output spectrum of ADC core B (c) Output spectrum of ADC core C (d) Output spectrum of ADC core D.

FIGURE 12. Output spectrum of EV8AQ160 8-bit TIADC with 800MHz input signal. The spurious tones are composed of linear mismatches, nonlinear distortions and nonlinear mismatch distortions.

Applying a single sinusoidal signal as the input to the system, which is given as

$$x(t) = |A|cos(\Omega_0 t + \angle A) = \frac{A}{2}(e^{j\Omega_0 t} + e^{-j\Omega_0 t}) \quad (80)$$

where A and Ω_0 are the amplitude and frequency of the input signal respectively. The frequency domain representation of $x(t)$ can be written as

$$X(j\Omega) = A\pi[\delta(\Omega - \Omega_0) + \delta(\Omega + \Omega_0)] \quad (81)$$

With (29) and (81), the output of TIADC can be obtained by

$$Y(j\Omega) = \frac{\pi}{MT_s} \frac{A^p}{2^{p-1}} \sum_{m=0}^{M-1} \sum_{k=-\infty}^{\infty} \sum_{p=0}^{P} \int_{-\infty}^{\infty} \cdots \int_{-\infty}^{\infty}$$

$$\times e^{-j2\pi k \frac{m}{M}} H_{m,p}(j\Omega_1, \cdots, j(\Omega - \sum_{i=1}^{l-1} \Omega_i - k\frac{2\pi}{MT_s}))$$

$$\times \prod_{i=1}^{p-1} [\delta(\Omega_i - \Omega_0) + \delta(\Omega_i + \Omega_0)]$$

$$\cdot \left[\delta(\Omega - k\frac{2\pi}{MT_s} - \sum_{i=1}^{p-1} \Omega_i - \Omega_0) \right.$$

$$\left. \times +\delta(\Omega - k\frac{2\pi}{MT_s} - \sum_{i=1}^{p-1} \Omega_i + \Omega_0) \right] d\Omega_1 \cdots d\Omega_{p-1}$$

$$(82)$$

Thus, the frequency of spurious tones generated by pth order nonlinearity in TIADC are located at $k\frac{\Omega_s}{M} \pm (p - 2i)\Omega_0(k = 0, \cdots, M-1, i = 0, \cdots, \lfloor\frac{p}{2}\rfloor)$ with $\Omega_s = \frac{2\pi}{T_s}$. Taking $p = 1$, we obtain frequency of the linear mismatch errors, i.e. $k\frac{\Omega_s}{M} \pm \Omega_0$, which is consistent with the conclusion in [13].

The second and third order nonlinear distortions are obtained by taking $k = 0$, i.e. $\pm(p - 2i)\Omega_0$. This types of distortions appear in single ADC systems. It can be seen that higher order nonlinearities superpose onto the same frequency bins as lower order nonlinearities. The second and third order nonlinear mismatch distortions are those with $k \neq 0$, which are extra distortions introduced by TIADC systems.
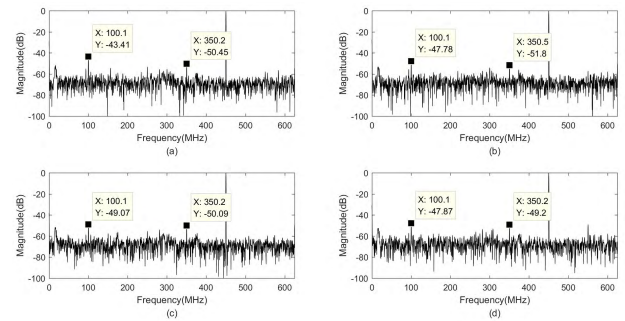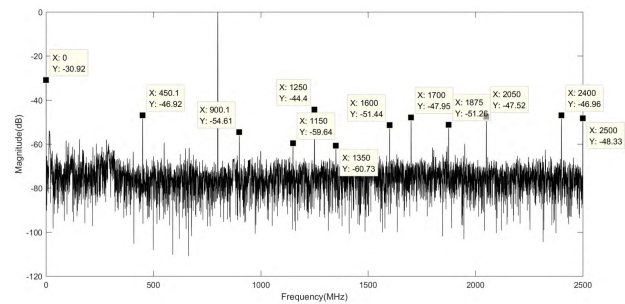
Fig.11 shows the output spectrum of each sub-ADC with 800MHz input signal. From the spectrum, it can be seen that only second and third order nonlinearities are obvious for EV8AQ160 while higher order nonlinearities have minor impact. For each sub-ADC, it samples at a sub-Nyquist rate hence the signal and nonlinear distortions are aliased for the sub-ADC. The aliased frequency for signal, second nonlinear distortion, third nonlinear distortion are located at 450MHz, 350MHz and 100MHz respectively. It can be seen from the figure that the second order and third order distortions differ significantly for each sub-ADC, thus will introduce nonlinear mismatch distortions in the output of the TIADC system.

The output spectrum of the TIADC system is shown in Fig.12. It can be seen that there are numerous spurious tones in the output spectrum. The offset mismatches are located at dc, 1250MHz and 2500MHz, with magnitude of -30.93dBc, −44.41dBc and −48.38dBc respectively. The linear mismatch errors are in 450MHz, 1700MHz and 2050MHz, which have magnitude of −46.93dBc, −47.54dBc and −47.94dBc respectively.

Apart from offset and linear mismatch errors, there are still numerous spurious tones significantly higher than the noise floor. The second and third order nonlinear distortions have magnitude of −51.43dBc and −46.97dBc respectively. The spurious tone located at 900MHz is caused by second order nonlinear mismatch errors, which has magnitude of −54.63dBc. The spurious tones located at 1150MHz and
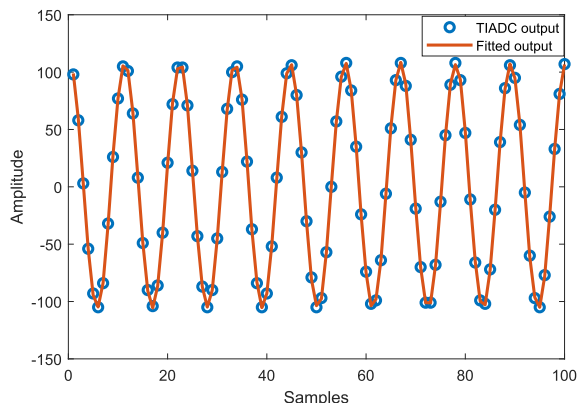
FIGURE 13. A sample of time-domain waveforms of TIADC output and modeled output. The circles represent the sampled output of the TIADC system. The solid line depicts the fitted output with Volterra-based model.

1350MHz are caused by third order nonlinear mismatch errors, which has magnitude of -59.69dBc and -60.81dBc.

From the experimental result, it can be seen that the location of those spurious tones are consistent with what we have derived from (82), which shows the effectiveness of the model we proposed. Besides, it can be concluded from experimental results that only considering offset and linear mismatches are not sufficient for cases where strong signals and weak signals exist together since distortions generated by strong signals may interfere with weak signals and hence calibration of the nonlinear mismatch errors is required.

Then the identification is required to demonstrate the performance of the proposed model. The identification method is given in section VI.A. However, the input signal is an analog signal in practice, which can not be used to form matrix X in (73) directly. The initial phase and amplitude can be obtained by minimizing root-mean-square error between output signal and sine signal with known frequency [20], [48]. The parameters of the sinusoidal signal can be obtained by four parameter-method proposed in IEEE Std 1241 [49].

The training signals are chosen as sinusoidal waves with 20 different frequencies within the bandwidth of the DUT with frequency spacing 100MHz. Then these signals are concatenated in time to form the novel training signal as in (79). We take 50 samples of each frequency and thus total 1000 samples in the identification, i.e. $N = 1000$ in (67). Since linear behaviors have greater impact on TIADC in practical situation, we set the linear memory length longer than the nonlinear memory length in the Volterra-based model. In the experiment, the nonlinear order is set as third as in simulation. The memory length of linear terms, second order terms and third order terms are set as 10, 4, 4 respectively.

The performance of the estimated model is verified by adopting signal with different frequency from training signal. We use a 450MHz signal as the validation signal. A sample of time-domain waveforms is shown in Fig.13. The circles represent the sampled TIADC output and solid line depicts the fitted output with estimated model parameters. The NMSE calculated for 450MHz signal with estimated model

is -39.2784 dB. It is seen that the proposed model is valid to describe phenomenon in real TIADC system. The NMSE can be improved further with more memory length in proposed model.

VII. CONCLUSIONS

In this paper, we have proposed the behavioral model to describe the dynamic nonlinearities in TIADC system based on Volterra series. We derive the hybrid TIADC model firstly, and then propose the discrete-time nonlinear equivalent model of TIADC, which makes it possible to make full use of the related existing derivations, conclusions and methodologies on discrete-time Volterra series. We also summarize some common special cases of Volterra series to provide a practical guideline for ADC and TIADC practitioners. The derivations in this paper give a theoretical foundation to use discrete-time Volterra series to model mixed-domain TIADC system. Then the nonlinear distortions can be calibrated using the proposed model, which will be our future directions.

REFERENCES

[1] J. Song, S. Tian, and Y.-H. Hu, "Analysis and correction of combined channel mismatch effects in frequency-interleaved ADCs," *IEEE Trans. Circuits Syst. I, Reg. Papers*, vol. 66, no. 2, pp. 655–668, Feb. 2019.

[2] Y. Zhao, Y. H. Hu, and J. Liu, "Random triggering-based sub-Nyquist sampling system for sparse multiband signal," *IEEE Trans. Instrum. Meas.*, vol. 66, no. 7, pp. 1789–1797, Jul. 2017.

[3] J. Song, S. Tian, Y.-H. Hu, and P. Ye, "Digital iterative harmonic rejection and image cancellation for LPF-less frequency-interleaved analog-to-digital converters," *IEEE Trans. Circuits Syst., II, Exp. Briefs*, to be published.

[4] W. C. Black and D. A. Hodges, "Time interleaved converter arrays," *IEEE J. Solid-State Circuits*, vol. 15, no. 6, pp. 1022–1029, Dec. 1980.

[5] Y.-C. Jenq, "Digital spectra of nonuniformly sampled signals: Fundamentals and high-speed waveform digitizers," *IEEE Trans. Instrum. Meas.*, vol. 37, no. 2, pp. 245–251, Jun. 1988.

[6] A. Petraglia and S. K. Mitra, "Analysis of mismatch effects among A/D converters in a time-interleaved waveform digitizer," *IEEE Trans. Instrum. Meas.*, vol. 40, no. 5, pp. 831–835, Oct. 1991.

[7] N. Kurosawa, H. Kobayashi, K. Maruyama, H. Sugawara, and K. Kobayashi, "Explicit analysis of channel mismatch effects in time-interleaved ADC systems," *IEEE Trans. Circuits Syst. I, Fundam. Theory Appl.*, vol. 48, no. 3, pp. 261–271, Mar. 2001.

[8] C. Vogel, "The impact of combined channel mismatch effects in time-interleaved ADCs," *IEEE Trans. Instrum. Meas.*, vol. 54, no. 1, pp. 415–427, Feb. 2005.

[9] D. Fu, K. C. Dyer, S. H. Lewis, and P. J. Hurst, "A digital background calibration technique for time-interleaved analog-to-digital converters," *IEEE J. Solid-State Circuits*, vol. 33, no. 12, pp. 1904–1911, Dec. 1998.

[10] S. M. Jamal, D. Fu, N. C. -J. Chang, P. J. Hurst, and S. H. Lewis, "A 10-b 120-Msample/s time-interleaved analog-to-digital converter with digital background calibration," *IEEE J. Solid-State Circuits*, vol. 37, no. 12, pp. 1618–1627, Dec. 2002.

[11] M. Seo, M. J. W. Rodwell, and U. Madhow, "Comprehensive digital correction of mismatch errors for a 400-Msamples/s 80-dB SFDR time-interleaved analog-to-digital converter," *IEEE Trans. Microw. Theory Techn.*, vol. 53, no. 3, pp. 1072–1082, Mar. 2005.

[12] T. H. Tsai, P. J. Hurst, and S. H. Lewis, "Bandwidth mismatch and its correction in time-interleaved analog-to-digital converters," *IEEE Trans. Circuits Syst. II, Exp. Briefs*, vol. 53, no. 10, pp. 1133–1137, Oct. 2006.

[13] C. Vogel and S. Mendel, "A flexible and scalable structure to compensate frequency response mismatches in time-interleaved ADCs," *IEEE Trans. Circuits Syst. I, Reg. Papers*, vol. 56, no. 11, pp. 2463–2475, Nov. 2009.

[14] H. Johansson, "A polynomial-based time-varying filter structure for the compensation of frequency-response mismatch errors in time-interleaved ADCs," *IEEE J. Sel. Topics Signal Process.*, vol. 3, no. 3, pp. 384–396, Jun. 2009.

[15] Y. C. Lim, Y. X. Zou, J. W. Lee, and S. C. Chan, "Time-interleaved analog-to-digital-converter compensation using multichannel filters," *IEEE Trans. Circuits Syst. I, Reg. Papers*, vol. 56, no. 10, pp. 2234–2247, Oct. 2009.

[16] K. M. Tsui and S. C. Chan, "New iterative framework for frequency response mismatch correction in time-interleaved ADCs: Design and performance analysis," *IEEE Trans. Instrum. Meas.*, vol. 60, no. 12, pp. 3792–3805, Dec. 2011.

[17] B. Xu and Y. Chiu, "Comprehensive background calibration of time-interleaved analog-to-digital converters," *IEEE Trans. Circuits Syst. I, Reg. Papers*, vol. 62, no. 5, pp. 1306–1314, May 2015.

[18] S. Singh, L. Anttila, M. Epp, W. Schlecker, and M. Valkama, "Analysis, Blind Identification, and Correction of Frequency Response Mismatch in Two-Channel Time-Interleaved ADCs," *IEEE Trans. Microw. Theory Tech.*, vol. 63, no. 5, pp. 1721–1734, May 2015.

[19] P. Satarzadeh, B. C. Levy, and P. J. Hurst, "Digital calibration of a nonlinear S/H," *IEEE J. Sel. Topics Signal Process.*, vol. 3, no. 3, pp. 454–471, Jun. 2009.

[20] P. Nikaeen and B. Murmann, "Digital compensation of dynamic acquisition errors at the front-end of high-performance A/D converters," *IEEE J. Sel. Topics Signal Process.*, vol. 3, no. 3, pp. 499–508, Jun. 2009.

[21] J. Goodman, B. Miller, M. Herman, G. Raz, and J. Jackson, "Polyphase nonlinear equalization of time-interleaved analog-to-digital converters," *IEEE J. Sel. Topics Signal Process.*, vol. 3, no. 3, pp. 362–373, Jun. 2009.

[22] Y. Wang, H. Johansson, H. Xu, and Z. Sun, "Joint blind calibration for mixed mismatches in two-channel time-interleaved ADCs," *IEEE Trans. Circuits Syst. I, Reg. Papers*, vol. 62, no. 6, pp. 1508–1517, Jun. 2015.

[23] Y. Wang, H. Johansson, and H. Xu, "Adaptive background estimation for static nonlinearity mismatches in two-channel TIADCs," *IEEE Trans. Circuits Syst. II, Exp. Briefs*, vol. 62, no. 3, pp. 226–230, Mar. 2015.

[24] Y. Wang, H. Xu, Q. Li, N. Li, and Z. Sun, "Estimation method for nonlinearity mismatch in time-interleaved analog-to-digital converters," in *Proc. IEEE Int. Symp. Circuits Syst. (ISCAS)*, Jun. 2014, pp. 2109–2122.

[25] H. Liu, Y. Wang, L. Nan, and H. Xu, "A calibration method for nonlinear mismatches in M-channel time-interleaved analog-to-digital converters based on Hadamard sequences," *Appl. Sci*, vol. 6, no. 11, p. 362, Nov. 2016.

[26] G. Huang, C. Yu, and A. Zhu,, "Analog assisted multichannel digital postcorrection for time-interleaved ADCs," *IEEE Trans. Circuits Syst., II, Exp. Briefs*, vol. 63, no. 8, pp. 773–777, Aug. 2016.

[27] J. B. Simoes, J. Landeck, and C. M. B. A. Correia, "Nonlinearity of a data-acquisition system with interleaving/multiplexing," *IEEE Trans. Instrum. Meas.*, vol. 46, no. 6, pp. 1274–1279, Dec. 1997.

[28] C. Vogel and G. Kubin, "Modeling of time-interleaved ADCs with nonlinear hybrid filter banks," *AEU-Int. J. Electron. Commun.*, vol. 59, no. 5, pp. 288–296, Jul. 2005.

[29] W. Wei, P. Ye, Y. Zhao, K. Yang, J. Gao, and W. Huang, "Explicit analysis of nonlinearities in time-interleaved ADC," *IEICE Electron. Express*, vol. 15, no. 11, p. 20180373, May 2018.

[30] V. Vito, *Theory of Functionals and of Integral and Integro-Differential Equations*. New York, NY, USA: DOVER 1959.

[31] M. Schetzen, *Theory of Functionals and of Integral and Integro-Differential Equations*. Hoboken, NJ, USA: Wiley 1980.

[32] C. M. Cheng, Z. K. Peng, W. M. Zhang, and G. Meng, "Volterra-series-based nonlinear system modeling and its engineering applications: A state-of-the-art review," *Mech. Syst. Signal Process.*, vol. 87, pp. 340–364, Mar. 2017.

[33] S. Boyd and L. Chua, "Fading memory and the problem of approximating nonlinear operators with Volterra series," *IEEE Trans. Circuits Syst.*, vol. 32, no. 11, pp. 1150–1161, Nov. 1985.

[34] T. Koh and E. Powers, "Second-order Volterra filtering and its application to nonlinear system identification," *IEEE Trans. Acoust., Speech, Signal Process.*, vol. 33, no. 6, pp. 1445–1455, Dec. 1985.

[35] S. Boyd, Y. Tang, and L. Chua, "Measuring volterra kernels," *IEEE Trans. Circuits Syst.*, vol. 30, no. 8, pp. 571–577, Aug. 1983.

[36] R. Yue, S. A. Billings, and Z.-Q. Lang, "An investigation into the characteristics of non-linear frequency response functions. Part 1: Understanding the higher dimensional frequency spaces," *Int. J. Control*, vol. 78, no. 13, pp. 1031–1044, Apr. 2005.

[37] A. V. Oppenheim, R. W. Schafer, and J. R. Buck, *Discrete-Time Signal Processing*. Englewood Cliffs, NJ, USA: Prentice-Hall, 1999.

[38] W. A. Frank, "Sampling requirements for Volterra system identification," *IEEE Signal Process. Lett.*, vol. 3, no. 9, pp. 266–268, Sep. 1996.

[39] H. Jeffreys and B. S. Jeffreys, *Methods of Mathematical Physics*, 3rd ed. Cambridge, U.K.: Cambridge Univ. Press, 1988.

[40] W. Greblicki, "Recursive identification of continuous-time Wiener systems," *Int. J. Control*, vol. 72, no. 11, pp. 981–989, 1999.

[41] E.-W. Bai and F. Minyue, "A blind approach to Hammerstein model identification," *IEEE Trans. Signal Process.*, vol. 50, no. 7, pp. 1610–1619, Jul. 2002.

[42] A. Y. Kibangou and G. Favier, "Wiener-Hammerstein systems modeling using diagonal Volterra kernels coefficients," *IEEE Signal Process. Lett.*, vol. 13, no. 6, pp. 381–384, Jun. 2006.

[43] J. Kim and K. Konstantinou, "Digital predistortion of wideband signals based on power amplifier model with memory," *Electron. Lett.*, vol. 37, no. 23, pp. 1417–1418, Nov. 2001.

[44] L. Ding *et al.*, "A robust digital baseband predistorter constructed using memory polynomials," *IEEE Trans. Commun.*, vol. 52, no. 1, pp. 159–165, Jan. 2004.

[45] D. R. Morgan, Z. Ma, J. Kim, M. G. Zierdt, and J. Pastalan, "A generalized memory polynomial model for digital predistortion of RF power amplifiers," *IEEE Trans. Signal Process.*, vol. 54, no. 10, pp. 3852–3860, Oct. 2006.

[46] A. Zhu, J. C. Pedro, and T. J. Brazil, "Dynamic deviation reduction-based volterra behavioral modeling of RF power amplifiers," *IEEE Trans. Microw. Theory Techn.*, vol. 54, no. 12, pp. 4323–4332, Dec. 2006.

[47] O. Hammi, F. M. Ghannouchi, and B. Vassilakis, "A compact envelope-memory polynomial for RF transmitters modeling with application to baseband and RF-digital predistortion," *IEEE Microw. Wireless Compon. Lett.*, vol. 18, no. 5, pp. 359–361, May 2008.

[48] C. A. Schmidt, O. Lifschitz, J. E. Cousseau, J. L. Figueroa, and P. Julián, "Methodology and measurement setup for analog-to-digital converter postcompensation," *IEEE Trans. Instrum. Meas.*, vol. 63, no. 3, pp. 658–666, Mar. 2014.

[49] *IEEE Standard for Terminology and Test Methods for Analog-to-Digital Converters*, Standard IEEE1241-2010, Jan. 2011.

[50] *Datasheet of EV8AQ160*. Accessed: Dec. 19, 2018. [Online]. Available: https://www.e2v.com/resources/account/download-datasheet/2291

[51] *Datasheet of SMA100A*. Accessed: Dec. 19, 2018. [Online]. Available: https://cdn.rohde−schwarz.com.cn/pws/dl_down-loads/

WENTAO WEI was born in Shanxi, China, in 1991. He received the B.S. degree in instrumentation and measurement science from the School of Automation Engineering, University of Electronic Science and Technology of China (UESTC), Chengdu, China, in 2014, where he is currently pursuing the Ph.D. degree with the Research Institution of Electronic Measurement and Instrument. His research interests include high-speed mixed-signal circuit design, digital signal processing, nonlinear systems, and machine learning.

PENG YE was born in Chengdu, China, in 1973. He received the B.S., M.S., and Ph.D. degrees from University of Electronic Science and Technology of China, in 1995, 2001, and 2010, respectively, where he is currently a Professor. His research interests include high-speed data acquisition, and signal processing and digital storage oscilloscope.

JINPENG SONG received the B.S. degree in instrumentation and measurement science from the School of Automation Engineering, University of Electronic Science and Technology of China, Chengdu, China, in 2013, where he is currently pursuing the Ph.D. degree in electrical engineering.

He was a Visiting Researcher with the University of Wisconsin–Madison, Madison, WI, USA, from 2016 to 2018. His research interests include the design and theory of digital, analog, and mixed-signal processing systems with special emphasis on communication systems and digital enhancement techniques for analog signal processing systems.

HAO ZENG was born in Dujiangyan, China, in 1979. He received the B.S., M.S., and Ph.D. degrees from University of Electronic Science and Technology of China, China, in 2002, 2005, and 2010, respectively, where he is currently an Associate Researcher. His research interests include high-speed and high-precision data acquisition, and signal processing and RF signal generator.

YU ZHAO was born in Shenyang, Liaoning, China, in 1993. He received the B.S. degree in electrics and information engineering from the School of Automation Engineering, University of Electronic Science and Technology of China, Chengdu, China, in 2015, where he is currently pursuing the Ph.D. degree in electrical engineering. His research interests include the design and theory of digital, analog, and mixed-signal processing systems and high-speed data acquisition systems.

• • •

JIAN GAO was born in Hebei, China, in 1993. He received B.S. degree from the University of Electronic Science and Technology of China (UESTC), Chengdu, China, in 2015, where he is currently pursuing the Ph.D. degree. His research interests include high-speed data acquisition, and signal processing and digital storage oscilloscope.